J Mater Sci

Energy materials

Covalent hybrid materials between polyoxometalates and organic molecules for enhanced electrochemical properties

Bo Huang[1,2,3], Degang Ke[1], Zhelun Xiong[1], Yu Wang[1], Kanghong Hu[1], Peng Jiang[2,*], Minghui Liang[2,*], Zicheng Xiao[1,*], and Pingfan Wu[1,*]

[1] *Institute of POM-Based Materials, Hubei Provincial Key Laboratory of Green Materials for Light Industry, Hubei University of Technology, Wuhan, China*
[2] *CAS Key Laboratory of Nanosystem and Hierarchical Fabrication, National Center for Nanoscience and Technology, Beijing, China*
[3] *University of Chinese Academy of Sciences, Beijing, China*

Received: 11 November 2019
Accepted: 26 January 2020

ABSTRACT

The organic functionalization of polyoxometalate (POM) clusters has exhibited increasing superiority for the rational excavation and design of advanced POM-based materials. The architectures of such inorganic–organic hybrids are just like "molecular Lego" toys by virtue of the intermolecular and/or intramolecular interactions. Although numerous novel hybrids have been reported by pioneers, the relationship between organic segments and supramolecular architectures is still ambiguous. In this paper, we focus on the influence from organic bridging ligand to the structural orientation of POM hybrid materials by X-ray diffraction, molecular simulation, and energy calculation. The results indicate that rigid organic bridging ligand possesses a much stronger tendency to form intermolecular interactions than flexible ligand and can improve the electrochemical performance for hydrogen evolution reaction.

Introduction

Polyoxometalates (POMs) are a family of metal oxide clusters derived from early transition metal (Mo, V, W, Nb, and Ta) salts being different from the traditional metal oxide crystals in structure, having intensive applications in catalysis and material science [1–4]. The principle POM clusters can be further fabricated into multiple topological architectures with regular shapes (such as circles, cages, spheres, and wheels) through the co-edge, co-angle, and coplanar conjunctions between the coordination of metal and oxygen atoms [5–9]. More importantly, POMs are promising building blocks for covalent inorganic–organic hybrid materials, exhibiting a different performance as a result of synergistic effects

---

Bo Huang and Degang Ke contributed equally to this work.

Address correspondence to E-mail: pjiang@nanoctr.cn; liangmh@nanoctr.cn; zichxiao@hotmail.com; pingfanwu-111@163.com

https://doi.org/10.1007/s10853-020-04404-0

between inorganic clusters and organic components [10–13]. The introduction of organic parts into such POM system has great influence on the crystalline structures and properties, which is important to the rational design of advanced POM hybrids [14–16]. To our best knowledge, the relationship between the structures of organic parts and the functions of hybrid materials has been systematically studied in the POM-based amphipathic systems and coordination systems, so that improved surfactant materials, heterogeneous catalysts, and selective cell adhesions were successfully fabricated benefiting from the revealed rules [17–20]. However, the non-covalent interactions in these systems are always regarded as appendix and used to be neglected. In fact, these non-covalent interactions can improve the dimensions of POM hybrid materials (such as chain, network, and framework), and their impacts to the structures and functions must be valued [21–23]. But unlike the coordination interaction, the existence of non-covalent interactions such as hydrogen bonds in an organic–inorganic hybrid system is usually hard to be predicted because it concerns multiple factors like the ligand structures, counter ions, and the courses of crystallization [7, 24–28]. Among these factors, we find that the choice of organic bridging ligand has a great influence on the non-covalent interactions of POM-based covalent hybrid materials, but no related research has been investigated; this is an obstacle for the further exploration.

As POMs possess a strong electron withdrawing effect and great steric hindrance [29], to choose a suitable bridging ligand during the construction of complicated POM-based hybrid materials is significant because of the following features: (1) bridging ligand can alleviate the electron withdrawing effect from the metal-based inorganic part by extending the organic chains; (2) remote functionalization can reduce the negative influence of the steric hindrance from POMs, especially for large organic molecules; (3) intermolecular and/or intramolecular interactions originating from the bridging ligands can lead to high-dimensional network or framework architectures, which are beneficial for the properties of the hybrid materials; (4) bridging ligands can also be useful tools to control the chemical environment or properties of the hybrids (for example, extending the organic conjugated system or increasing/reducing the hydrophilia of the hybrid). Recently, Cronin and our group have employed succinyl group as a bridging ligand in Anderson-type and Lindqvist-type POMs, respectively, to achieve various inorganic biomolecules with enhanced antitumor activities [30, 31]. But as the relationship between the bioactivities and the structure remained unclear, it is not beneficial for the further design of POM-based drugs with higher effect. During the later researches, other types of bridging ligands, especially for the rigid bridging ligands, have been successfully grafted onto the POMs, exhibiting fruitful multidimensional inorganic–organic architectures [32, 33]. However, how the flexible or rigid organic bridging ligands influence the supramolecular assemblies and properties of POM hybrid materials is still ambiguous. Thus, to reveal the secret in the influence of bridging ligands on the supramolecular architectures and target functions is a significant and pioneering work towards the rational design of POM-based hybrid materials.

In this paper, Lindqvist-type polyoxovanadate (POV) is chosen as the platform (Fig. 1) to explore the influences from the flexible/rigid organic bridging ligands to the architectures and functions because of the following advantages: (1) This kind of POM possesses a compact structure with low molecular charges, providing a simple platform for further researches; (2) it is convenient to conduct organic functionalization on this platform by virtue of the tris-alkoxo (TRIS) ligands {$(HOCH_2)_3CR$}; (3) feasible crystallization with regular technologies can provide possibility to study the structures on molecular/atomic level by single-crystal X-ray diffraction [19, 34–38]. We select a typical flexible bridging ligand (succinyl ligand) and a rigid bridging ligand (phthalyl ligand) to link with POVs, respectively. Cyclopropylamine, with a simple stable molecular orientation, is chosen as the terminal ligand. We explore the structural characteristics of the obtained two compounds by single-crystal X-ray diffraction, molecular simulation, energy calculation, and a series of spectra technologies. This is the first time to investigate how the flexible/rigid bridging ligands influence the non-covalent interactions in the POM hybrid material. In order to reveal the relationship between such interactions and the electrochemical properties of hybrid materials, we also study the electrocatalytic properties of the two compounds for hydrogen evolution reaction (HER). HER is one of the most clean routes to produce hydrogen and to alleviate the pressure of energy crisis [39]. Some POM

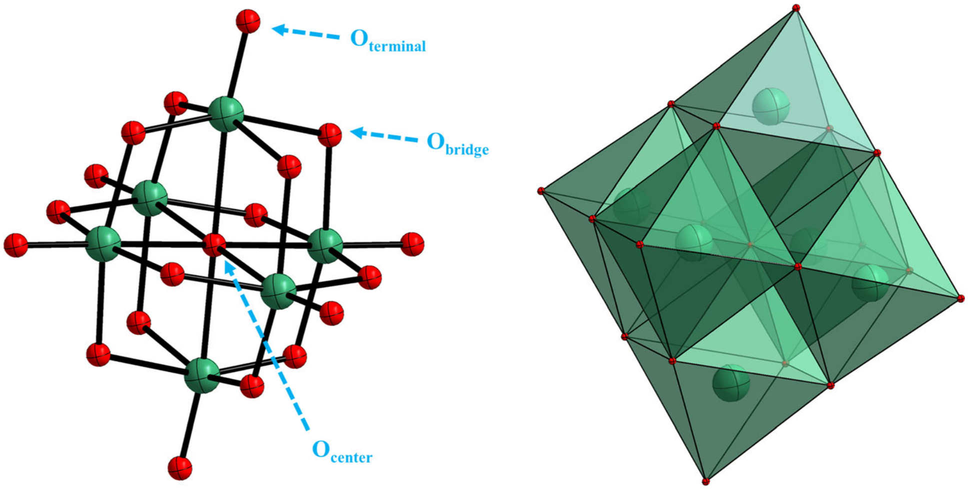

Figure 1 Ball-and-stick model (left) and the polyhedral model (right) of the Lindqvist-type hexavanadate platform. Green spheres: V atoms; red spheres: O atoms.

materials possessing multiple-electron transfer ability have been identified to be promising HER electrocatalysts in previous reports [40], and this work is the first time to investigate the potential application of Lindqvist-type POVs for HER. The results indicate that POV hybrid containing rigid bridging ligands delivers an enhanced electrochemical property than that with flexible one, giving a new mind for the programmatic construction of covalent POM-based inorganic–organic hybrid materials and a promising idea to design novel electrocatalysts.

Experimental

Materials

All chemicals were purchased from commercial sources and used without further purification except for CH_3CN, which has been dried by distillation in the presence of CaH_2 prior to use. $NaVO_3$ (analytical reagent,AR) was purchased from Shanghai Macklin Biochemical Co. Ltd. CH_3CN (AR), concentrated hydrochloric acid (12 M), pentaerythritol (AR), tetrabutylammonium bromide (AR), succinic anhydride (AR), *o*-phthalic anhydride (AR), triethylamine (AR), ethyl acetate (AR), and cyclopropylamine (AR) were purchased from Sinopharm Chemical Reagents Co. Ltd. 4-Dimethylaminopyridine (DMAP) and 2-ethoxy-1-ethoxycarbonyl-1,2-dihydroquinoline (EEDQ) were purchased from Aladdin Reagents Co. Ltd.

Preparation of the carboxyl-containing POV platforms

Two types of carboxyl-containing POV platforms, $(Bu_4N)_2\{V_6O_{19}[(CH_2)_3CCH_2OOCCH_2CH_2COOH]_2\}$ and $(Bu_4N)_2\{V_6O_{19}[(CH_2)_3CCH_2OOCC_6H_4COOH]_2\}$, were prepared according to the previous literature [33, 41]. Typically, 26.0 g $NaVO_3$ was dissolved into 100 mL deionized water and the pH value of the solution was adjusted to 2.0 by adding diluted hydrochloric acid (1 M). The mix was stirred at 80 °C for 2 days. Then, the dark red solution was filtrated and the filtrate was added to a solution of tetrabutylammonium bromide (52.0 g tetrabutylammonium bromide dissolved in 50 mL deionized water). After filtration, orange solid was obtained and washed by deionized water for 3 times, so that the hydroxyl-containing POV platform $(Bu_4N)_2\{V_6O_{19}[(CH_2)_3CCH_2OH]\}_2$ was collected after drying in vacuum drying oven. Later, mild esterification was conducted to prepare the carboxyl-containing POV platforms through reported method [42]. A mix of $(Bu_4N)_2\{V_6O_{19}[(CH_2)_3CCH_2OH]\}_2$ (2.0 g), succinic anhydride (0.5 g), trimethylamine (0.32 g), DMAP (0.008 g), and 50 mL CH_3CN was stirred and heated at 50 °C for 1 day. After filtration and evaporation, the product of $(Bu_4N)_2\{V_6O_{19}[(CH_2)_3CCH_2OOCCH_2CH_2COOH]_2\}$ was obtained. Similarly, $(Bu_4N)_2\{V_6O_{19}[(CH_2)_3CCH_2OOCC_6H_4COOH]_2\}$ was synthesized by adding *o*-phthalic anhydride rather than succinic anhydride with the same ratio. These two types of bridging ligand-containing POV platform were successfully prepared for later usage.

Synthesis of compound 1

$(Bu_4N)_2\{V_6O_{19}[(CH_2)_3CCH_2OOCCH_2CH_2COOH]_2\}$ (0.146 g, 0.1 mmol) was dissolved in 20 ml anhydrous acetonitrile. EEDQ (0.059 g, 0.24 mmol) was added to the solution and reacted for 30 min, cyclopropylamine (0.012 g, 0.2 mmol) was then added, and the mixture was stirred at 60 °C for one day. After reaction, the red transparent solution was cooled to room temperature and the solvent was evaporated. The residues were washed with ethyl acetate until they became powder. Red crystals of the product were obtained by dissolving the powder in an acetonitrile/water mixture and allowed to stand for 3 days in about 76% yield. ^1H NMR (400 MHz, d_6-DMSO, ppm): 7.916 (d, NH, 2H), 4.924 (s, CH2, 12H), 3.936 (d, CH2, 4H), 3.202 (m, CH2, 16H), 3.182 (m, CH, 2H), 2.479 (d, CH2, 4H), 2.283 (t, CH2, 4H), 1.604 (m, CH2, 16H), 1.352 (m, CH2, 16H), 0.963 (t, CH3, 24H), 0.602 (m, CH2, 4H), 0.380 (m, CH2, 4H); FT-IR spectrum (cm^{-1}, KBr pullets): 2960 (m), 2873 (m), 1731 (s), 1677 (s), 1467 (m), 1379 (w), 1247 (w), 1168 (s), 1134(s), 1063 (s), 952 (vs), 806 (s), 720 (s), 583(m); UV–Vis (MeCN): λ_{max} = 358 nm; Elemental analysis: C 43.21%, N 3.36%, H 7.02% (in theory: C 43.65%, N 3.64%, H 6.93%).

Synthesis of compound 2

$(Bu_4N)_2\{V_6O_{19}[(CH_2)_3CCH_2OOCC_6H_4COOH]_2\}$ (0.156, 0.1 mmol) was dissolved in 20 ml anhydrous acetonitrile. EEDQ (0.059 g, 0.24 mmol) was applied as catalyst to improve the reactive activity of carboxyl groups. After activation for 30 min, cyclopropylamine (0.012 g, 0.2 mmol) was added and stirred at 60 °C for one day. After that, the red transparent solution was cooled to room temperature and the solvent was evaporated. Then, the obtained solids were washed with ethyl acetate until they became powder. The products were recrystallized in an acetonitrile/water mixture solvent for 3 days to collect red crystals in about 68% yield. ^1H NMR (400 MHz, d_6-DMSO, ppm): 8.597 (d, NH, 2H), 7.892(d, aromatic, 2H), 7.774 (d, aromatic, 2H), 7.692 (t, aromatic, 2H), 7.629 (t, aromatic, 2H), 5.073 (s, CH2, 12H), 4.202 (s, CH2, 4H), 3.292 (m, CH2, 16H), 3.271 (m, CH, 2H), 1.689 (m, CH2, 16H), 1.421 (m, CH2, 16H), 1.053 (t, CH3, 24H), 0.800 (m, CH2, 4H), 0.654 (m, CH2, 4H); FT–IR spectrum (cm^{-1}, KBr pullets): 2961 (m), 2874 (m), 1732 (s), 1660 (s), 1471 (s), 1267 (s), 1129 (s), 1058 (s), 953 (vs), 809 (s), 720 (s), 582(s); UV–Vis (MeCN): λ_{max} = 353 nm; Elemental analysis: C 45.64%, N 3.57%, H 6.56% (in theory: C 46.90%, N 3.42%, H 6.64%).

Instrumental characterizations

^1H NMR spectra were recorded on an AV400 NMR spectrometer with DMSO-d_6 solvent. UV–Vis absorption spectra were recorded on a SHIMADZU UV-2700 spectrophotometer. Single-crystal X-ray diffraction data were collected on a SuperNova diffractometer. FT-IR spectra were recorded on a Nicolet iS50 infrared spectrometer using KBr pellets. TGA were performed using a METTLER TOLEDO TGA apparatus at a rate of 10 K min^{-1} under an N_2 stream. Powder X-ray diffraction data were measured with a PANalytical Empyrean Diffractometer. TEM was conducted on Tecnai G2 F20 U-TWIN. XPS data were measured with a PH15000 VersaProbe III spectrometer. High-resolution electrospray ionization mass spectra (HR–ESI–MS) were recorded on an Orbitrap high-resolution electrospray ionization mass spectrometry. Molecular simulations and energy calculations were done on Gaussian computer with b3lyp/6-311 g(d,p) model. The electrochemical experiments were tested on a Multi Autolab M204 workstation (Metrohm, Switzerland) with a three-electrode system. A mix of sample (1.5 mg) and acetylene black (8 mg) was dispersed in a mix solution of 500 μL of acetonitrile and 5% Nafion solution (10:1 *v*/*v*). After ultrasonic dispersion for 1 h, 5 μL homogeneous suspension was dropped on a glassy carbon electrode (GCE, 3 mm in diameter), which was applied as working electrode. A carbon rod was employed as the counter electrode and a saturated calomel electrode (SCE) as the reference electrode. The linear sweep voltammetry (LSV) tests were conducted in 0.5 M H_2SO_4 at a scan rate of 5 mV s^{-1} after cycling 100 cycles to stabilize the current with 95% *IR* compensation.

Results and discussion

The stepwise functionalization of POVs is based on the active organic group (carbonyl group) in the bridging ligands. With mild esterification and amidation, compounds 1 and 2 were successfully synthesized with the same terminal ligand but two types of bridging ligands (Scheme 1). Fortunately, the crystals of the two complexes were obtained, the quality of which were good enough for single-crystal X-ray diffraction to determine their inherent structures (detailed diffractive data in Table 1). The ORTEP and polyhedral diagrams of compounds 1 and 2 are shown in Figures S1–S2. Tables S1–S4 display their bond distances and angles. The parent structure of the hybrid anions in both compounds is a typical Lindqvist-type octahedral cluster consisting of six vanadium atoms and nineteen oxygens. Two TRIS ligands are linked to the inorganic core by substituted six bridging oxygens from two opposite sides of the octahedron. The organic segments of both hybrid anions are ended with a cyclopropyl ring. The main difference between the two hybrid anions is the bridging ligands. In compound 1, the pentaerythritol ligand and the cyclopropyl ring are linked by a flexible succinyl ligand. On the other hand, phthalyl ligand delivers a rigid bridge for the further organic linkage in compound 2. The amidic C-N bond between the bridging ligand and the cyclopropylamino group in compound 2 is a little longer than that in compound 1 because of the conjugative effect between benzene ring and carbonyl group. (These bond lengths are consistent with the stretching vibration peaks in FT–IR data, Figure S8 and Table S7.)

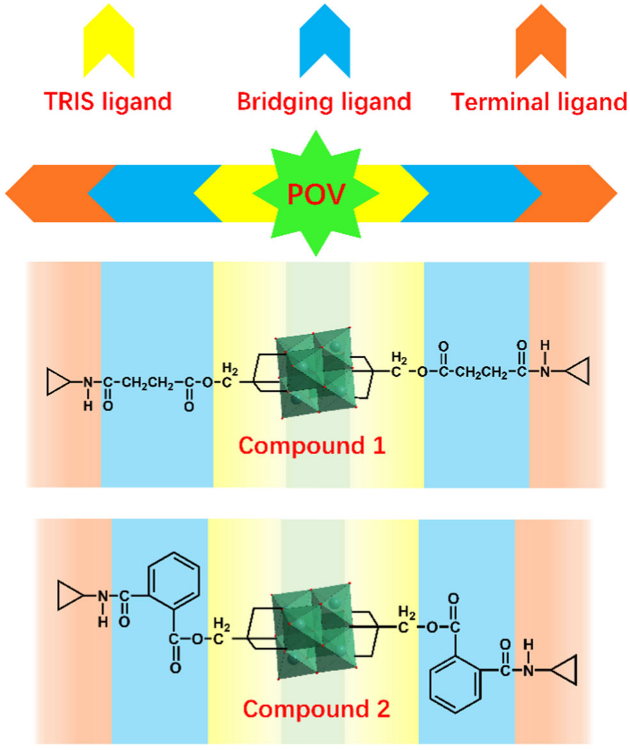

Scheme 1 Stepwise functionalization of compounds 1 and 2.

Towards the rational design of supramolecular inorganic–organic hybrid materials, one key problem is how to predict intermolecular interactions such as hydrogen bonds during molecular design. Although supramolecular chemistry has made great progress in the past decade, the relationship between guests, hosts, and intermolecular interactions is still ambiguous, making great drawbacks in design of new supramolecular hybrid materials. According to the previous reports, the assemblies of POV hybrids can be influenced or controlled by coordination [43], hydrogen bond (even V···H bond) [44], organic ligand [45], and the solvent [46]. For example, Cronin provided the comparative data of tris-functionalized Anderson-type polyoxomolybdates with succinyl or phthalyl ligands [32]. However, there is no interaction between these hybrid molecules, and the clusters are only wrapped by Bu_4N^+ cations. However, when they attached tetraphenylphthalyl ligands to the tris-functionalized polymolybdates, intermolecular hydrogen bonds can be found which arranged the hybrids to a 2D network.

In our previous work, we also studied the influence of the carboxylate ligands on the non-covalent interactions in the tris-functionalized Lindqvist-type hexavanadates. Different from Anderson-type polymolybdates, the hexavanadates with succinyl ligands showed intramolecular hydrogen bonds between the terminal carboxyl groups and the terminal oxygens of the cluster, while the phthalyl ligand derivative could form 2D network through intermolecular hydrogen bonds. Interestingly, when tetrahydrophthalyl ligand was employed as a bridging ligand, two types of hydrogen bonds (intermolecular and intramolecular) were observed in the hybrid anion because the cyclohexenyl ring was flexible and able to rotate [33]. These examples demonstrated that the supramolecular interactions can be regulated by organic ligands. In this work, the packing diagrams of both compounds are shown in Figure S3-S5. For compound 1, the inherent intramolecular hydrogen bonds are destroyed after the modification with cyclopropylamine, and no hydrogen bonds interaction can be observed in the crystal packing (Fig. 2). However, hydrogen bonds can still be found in the packing structures of compound 2 between amide groups and the terminal oxygens of the nearby cluster with the distance of

Table 1 Crystal data and structure refinement for compound 1 and compound 2

	Compound 1	Compound 2
Empirical formula	$C_{56}H_{106}N_4O_{25}V_6$	$C_{64}H_{108}N_4O_{25}V_6$
CCDC number[1]	1905161	1905160
Formula weight	1541.08	1639.18
Temperature/K	100.2(9)	100.00(11)
Crystal system	Monoclinic	Triclinic
Space group	*C*2/*c*	*P*-1
a/Å	30.4688(16)	11.0248(7)
b/Å	11.4542(2)	13.5796(8)
c/Å	23.2595(14)	14.7822(9)
α/°	90	101.111(5)
β/°	122.863(8)	105.035(5)
γ/°	90	113.738(6)
Volume/Å^3	6818.5(8)	1842.7(2)
Z	4	1
ρ_{calc}mg/mm^3	1.501	1.477
μ/mm^{-1}	7.298	0.808
F(000)	3232.0	858.0
Crystal size/mm^3	0.4 × 0.2 × 0.1	0.3 × 0.2 × 0.08
Radiation	MoKα (λ = 1.54184)	MoKα (λ = 0.71073)
2Θ range for data collection	7.86–153.704°	6.75–54.998°
Index ranges	$-32 \le h \le 38$	$-13 \le h \le 14$
	$-14 \le k \le 12$	$-17 \le k \le 17$
	$-28 \le l \le 29$	$-19 \le l \le 18$
Reflections collected	13686	17393
Independent reflections	$R_{int} = 0.0249$	$R_{int} = 0.0322$
	$R_{sigma} = 0.0319$	$R_{sigma} = 0.0581$
Data/restraints/parameters	6948/13/531	8459/0/462
Goodness of fit on F^2	1.045	1.050
Final *R* indexes [$I \geq 2\sigma$ (I)]	$R1 = 0.0666$, $wR2 = 0.1998$	$R1 = 0.0692$, $wR2 = 0.1827$
Final *R* indexes [all data]	$R1 = 0.0775$, $wR2 = 0.2149$	$R1 = 0.0990$, $wR2 = 0.2034$
Largest diff. peak/hole/e Å^{-3}	0.88/− 0.51	1.36/− 0.52

[1] CCDC represents the Cambridge Crystallographic Data Centre

2.1698(2) Å between the acceptor and the hydrogen (Fig. 3) and the clusters are arranged into 1D chain architectures by these interactions.

We summarized the reported hexavanadate hybrids with similar structure in Table 2. It can be seen that not all the hexavanadate hybrids with a flexible succinyl bridging ligand can form intermolecular interactions. Their supramolecular assemblies might be influenced by the following factors: (1) intramolecular hydrogen bonds would be eliminated when the carboxyl group is organically modified; (2) the types of functional groups (such as simple alkyl chains, amino acid ester, and aromatic derivatives) would affect the intermolecular interactions, including the dimensions of the supramolecular assemblies; (3) extra interactions, such as halogen bonds, would make the polyanions arrange closely and increase the dimensions of assemblies (from 1D chain, 2D network to 3D framework); (4) π–π interaction is hard to be established between the benzene-derived hexavanadates because of the steric hindrance from the inorganic octahedrons, also hard for Anderson-type polymolybdates [32]. Meanwhile, the POV hybrid with rigid phthalyl bridging ligand is all inclined to form intermolecular hydrogen bonds.

To explore whether rigid bridging ligand can pile up the POV hybrid anions more close than flexible bridging ligand, we try to employ molecular simulations to verify this question. Different from the reported terminal ligands, cyclopropylamine with a closed triangle ring structure is suitable for the comparison of such two types of bridging ligands.

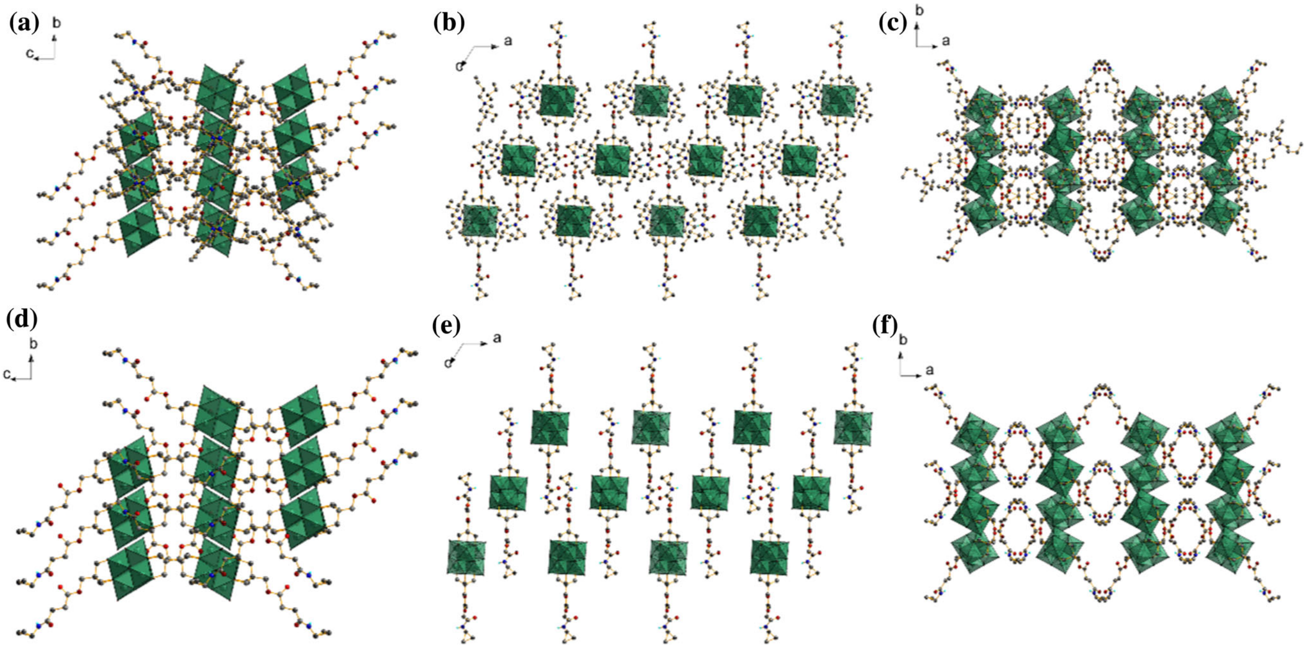

Figure 2 Packing diagrams of the compound 1 **a–c** viewed from different directions and the TBA$^+$ are hided for clarity in **d–f**. Green spheres: V atoms, red spheres: O atoms, grey spheres: C atoms, blue spheres: N atoms, light blue spheres: H atoms. Green octahedron represents the hexavanadate cluster. Thermal ellipsoids are drawn at 50% probability level.

Thus, we selected the packing models of compounds 1 and 2 as dimer templates for molecular simulations (Figure S6, S7 and Table S5, S6) and the binding energy of the two compounds in both two templates was calculated (Fig. 4). For compound 1, the binding energy was 0.129397 a.u. in its inherent crystal arrangement, but the binding energy increased to 1.458036 a.u. when the architecture of compound 1 was simulated to assembly through intermolecular hydrogen bonds (as the configuration of compound 2 with same acceptors and donors in hydrogen bonds). Owing to the greater degree of freedom, the succinyl ligands in compound 1 were much more flexible and the extra intermolecular hydrogen bonds interactions were difficult to be established, so that the simulative architecture was unstable and possessed higher dimer energy. On the other hand, the binding energy of the dimer structures of compound 2 was 0.087459 a.u., but the binding energy shifted to 2.298632 a.u. when the intermolecular hydrogen bonds were eliminated in simulation. These results indicate that the rigid phthalyl ligand delivers a closer packing model than the flexible succinyl ligand, and hydrogen bonds are more easily established in virtue of such packing model. However, the POV hybrid with flexible succinyl ligand might need extra conditions to form supramolecular polymers, such as the steric influence from the terminal ligands (e.g. ester groups or halogen atoms in the terminal functional groups) [47, 48].

The structures of compounds 1 and 2 were also investigated by a series of spectroscopic technologies. FT-IR spectra with the assignments of the peaks are shown in Figure S8 and Table S7, respectively. In both the two hybrids, the stretching vibrations of V–O$_{\text{terminal}}$, V–O$_{\text{bridge}}$, and V–O$_{\text{alkoxy}}$ gave absorption peaks around 953 cm^{-1}, 806 cm^{-1}, and 720 cm^{-1}, respectively. These results were consistent with the literature and indicated that the parent POV cluster has not been destroyed after such stepwise organic functionalization [42]. The strong and sharp absorption peaks around 1730 cm^{-1} and 1670 cm^{-1} corresponded to the stretching vibrations of carbonyl groups in the ester group and amide group, respectively. Owing to the conjugative effect from the aromatic benzene ring, the wavenumber of amide group in compound 2 was weaken (1660 cm^{-1}) in comparison with that of compound 1 (1677 cm^{-1}). This result is also consistent with the single-crystal data. UV–Vis spectra (Figure S9) show that both two compounds exhibited absorption peak with maximum wavelength around 360 nm, corresponding to the $\pi \rightarrow \pi^*$ transitions of V=O$_{\text{terminal}}$ in the POV parent structure. Figure S10 and Table S8 show the ^{1}H NMR spectra

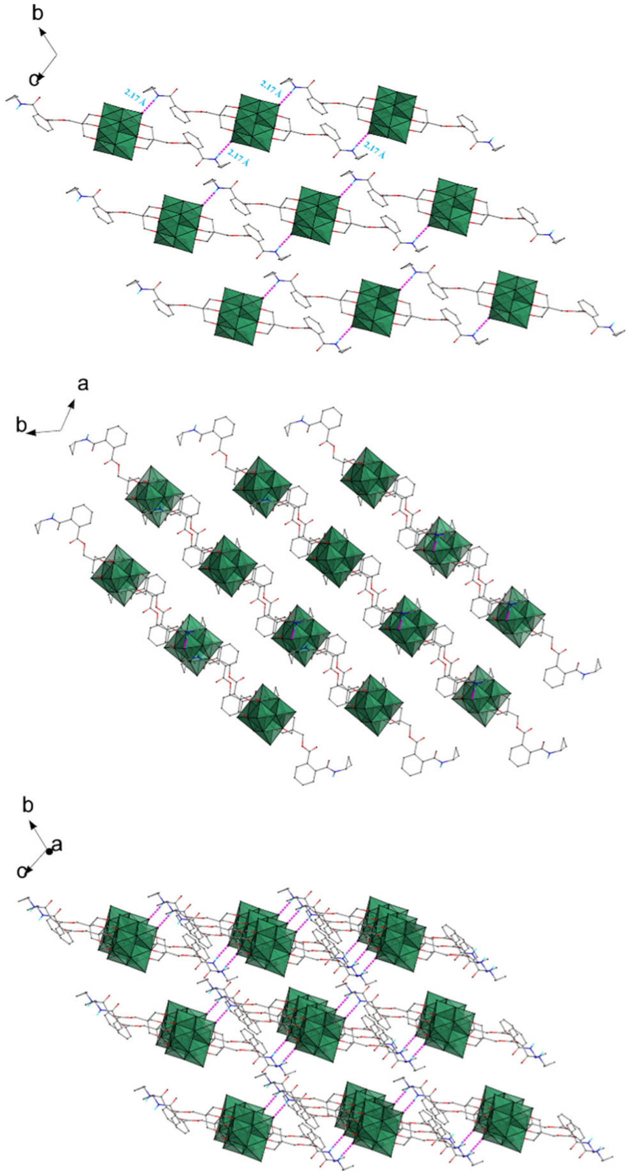

Figure 3 Packing diagrams viewed along different axes and supramolecular assemblies of compound 2 originating from intermolecular hydrogen bonds. All hydrogen atoms except N–H are hided for clarity.

and chemical shifts of the two compounds. All signals of the protons were exactly assigned, and the integrations were consistent with the assumed structures. Together with the results of high-resolution electrospray ionization mass spectra, an efficient technology to verify the molecular information of POM systems [49], the molecular formulas of the two compounds were confirmed and kept consistent with the single-crystal X-ray diffraction data (Fig. 5 and Table S9, S10).

In order to verify the purity of the hybrids, powder X-ray diffraction was conducted and the patterns were in accord with the simulated patterns derived from the single-crystal X-ray diffraction data (Fig. 6). However, the lattice structures of these two hybrids were hardly observed by transmission electron microscope (Figure S11). Energy-dispersive X-ray spectra of the two hybrids are demonstrated in Figure S12, the elemental signal and molar ratio were also consistent with the single-crystal X-ray diffractive data. X-ray photoelectron spectroscopy was applied to further elucidate the composition of the hybrids (Fig. 7). Both of the V2*p* spectra of these two compounds can only be fitted to a single peak so that all the vanadium atoms in the structures were in the same chemical environments. The electron binding energies at 515.9 eV (2*p* 3/2) and 523.2 eV (2*p* 1/2) for both two compounds indicated that all vanadium atoms were with highest +5 valence state (V^V).

The thermal stabilities of the hybrids were investigated by thermogravimetric analysis. As shown in Figure S13, both two hybrids exhibited a two-stage weight loss. The first weight loss occurred at 200 °C corresponding to the pyrolysis of organic ligands, while the weight loss at 500 °C was caused by the collapse of inorganic POV cluster. The well thermal stabilities of these compounds can ensure their further utilization.

Most of the reported POV hybrids are composited of vanadium atoms with highest valence state, possessing strong oxidizing ability and exhibiting excellent electrochemical performance in ascorbic acid oxidation, supercapacitor, redox flow batteries, sodium-ion battery, and oxygen reduction reaction [50–56]. According to a series of explorations of the POV-based organic derivatives by Monakhov's and our previous efforts, the organic functionalization of POVs will actually affect their electrochemical performances [57–60]. To explore the possible applications of the POV hybrids in electrocatalytic HER, liner sweep voltammetry (LSV) was tested with a three-electrode configuration under acid condition (Fig. 8a). It was apparent that POV-modified electrodes can dramatically improve the performance in comparison with glassy carbon electrode and acetylene black-modified electrode. Compound 2 delivered electrocatalytic performance with overpotential of 670 mV at 10 mA cm^{-2}, which was much lower than compound 1 and POV parent (with overpotential of 807 mV and 842 mV at 10 mA cm^{-2},

Table 2 Summary of the relative reported hexavanadate hybrids with phthalyl and succinyl bridging ligands

Anion formula	CCDC number	Crystal system	Space group	Interaction	Assembly	Ref.
$[V_6O_{13}\{(OCH_2)_3CCH_2OOCCH_2CH_2COOH\}_2]^{2-}$	1425970	Monoclinic	$P2_1/c$	Intramolecular hydrogen bonds (-COOH···O_t-V)		[41]
$[V_6O_{13}\{(OCH_2)_3CCH_2OOCCH_2CH_2CONHCH_2CH_2CH_3\}_2]^{2-}$	1425971	Monoclinic	$P2_1/n$	Not found	Not found	[41]
$[V_6O_{13}\{(OCH_2)_3CCH_2OOCCH_2CH_2CONHCH_2(CH_2)_2CH_3\}_2]^{2-}$	1425972	Monoclinic	$C2/c$	Not found	Not found	[41]
$[V_6O_{13}\{(OCH_2)_3CCH_2OOCCH_2CH_2CONHCH_2CH = CH_2\}_2]^{2-}$	1425973	Monoclinic	$P2_1/n$	Not found	Not found	[41]
$[V_6O_{13}\{(OCH_2)_3CCH_2OOCCH_2CH_2CONHC_6H_4Cl\text{-}p)\}_2]^{2-}$	1855376	Monoclinic	$P2_1/n$	Hydrogen bonds	1D chain	[47]
$[V_6O_{13}\{(OCH_2)_3CCH_2OOCCH_2CH_2CONHC_6H_4Br\text{-}p)\}_2]^{2-}$	1855377	Triclinic	*P-1*	Hydrogen and halogen bonds	3D framework	[47]
$[V_6O_{13}\{(OCH_2)_3CCH_2OOCCH_2CH_2CONHC_6H_4I\text{-}p)\}_2]^{2-}$	1855378	Triclinic	*P-1*	Hydrogen and halogen bonds	3D framework	[47]
$[V_6O_{13}\{(OCH_2)_3CCH_2OOC(C_6H_4)COOH\}_2]^{2-}$	1484789	Monoclinic	$P2_1/c$	Hydrogen bonds	2D network	[33]
$[V_6O_{13}\{(OCH_2)_3CCH_2OOC(C_6H_4)CONHCH_2CH_2CH_3\}_2]^{2-}$	1541544	Monoclinic	$P2_1/n$	Hydrogen bonds	2D network	[21]
$[V_6O_{13}\{(OCH_2)_3CCH_2OOC(C_6H_4)CONHCH_2CH = CH_2\}_2]^{2-}$	1541545	Monoclinic	$P2_1/n$	Hydrogen bonds	2D network	[21]
$[V_6O_{13}\{(OCH_2)_3CCH_2OOC(C_6H_4)CONHCH_2CH_2CH_2CH_3\}_2]^{2-}$	1541546	Triclinic	*P-1*	Hydrogen bonds	1D chain	[21]
$[V_6O_{13}\{(OCH_2)_3CCH_2OOC(C_6H_4)CONHC_6H_5\}_2]^{2-}$	1569404	Triclinic	P-1	Hydrogen bonds	1D chain	[21]
$[V_6O_{13}\{(OCH_2)_3CCH_2OOCCH_2CH_2CONHCH(CH_2)_2\}_2]^{2-}$	1905161	Monoclinic	$C2/c$	Not found	Not found	This work
$[V_6O_{13}\{(OCH_2)_3CCH_2OOC(C_6H_4)CONHCH(CH_2)_2\}_2]^{2-}$	1905160	Triclinic	*P-1*	Hydrogen bonds	1D chain	This work

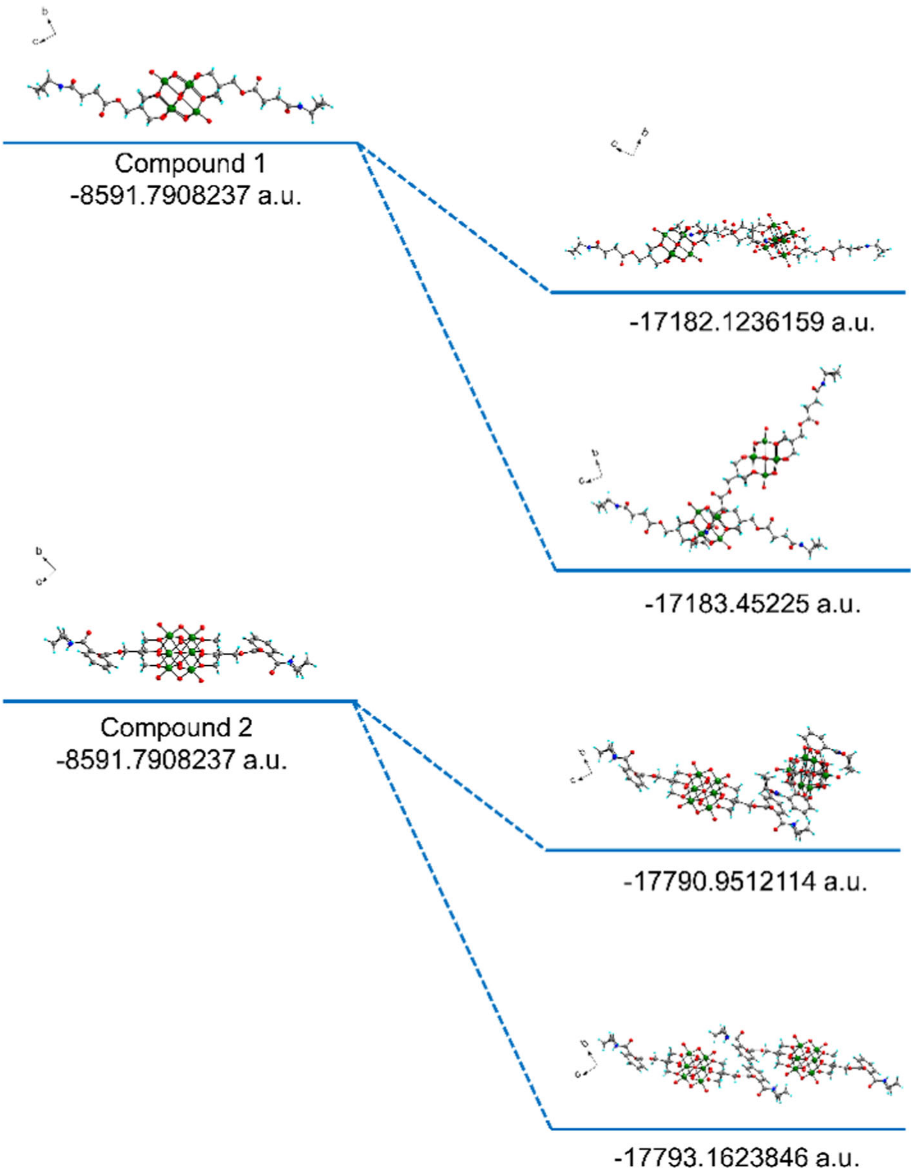

Figure 4 Molecular simulations and energy calculations of compounds 1 and 2, respectively.

respectively). More importantly, compound 2 also exhibited better performance at high current densities (Fig. 8b). As previous literature reported, POM-based organic frameworks exhibited high catalytic performance owing to the strong interactions between POM segments [61–64]. It can be assumed that the intermolecular interactions in compound 2 would also be beneficial for the electrocatalytic activity than the flexible bridging ligand derived one. The Tafel slopes of these novel electrocatalysts are shown in Fig. 8c. Compound 2 exhibited the lowest Tafel slope (83 mV dec^{-1}) than POV parent (126 dec^{-1}) and compound 1 (119 dec^{-1}), indicating that compound 2 possessed the fastest electrocatalytic kinetics than the other hybrid materials. This result also showed that the rate-limiting step for compound 2 was Heyrovsky step, while compound 1 and POV parent followed Volmer step as the rate-limiting step in HER [65–67]. Additionally, the electrochemical active surface areas were evaluated by double-layer capacitance (C_{dl}) through cyclic voltammetry at different scan rates (Figure S14). The C_{dl} values of POV parent, compound 1, and compound 2 were 0.59 mF cm^{-2}, 0.77 mF cm^{-2}, and 1.33 mF cm^{-2}, respectively (Fig. 8d). This result indicated that rigid bridging ligand provided enhanced electrochemical active surface area than that of flexible bridging ligand, and this was also the reason why compound 2 possessed the enhanced electrocatalytic performance. On the one hand, the larger electrochemical active surface

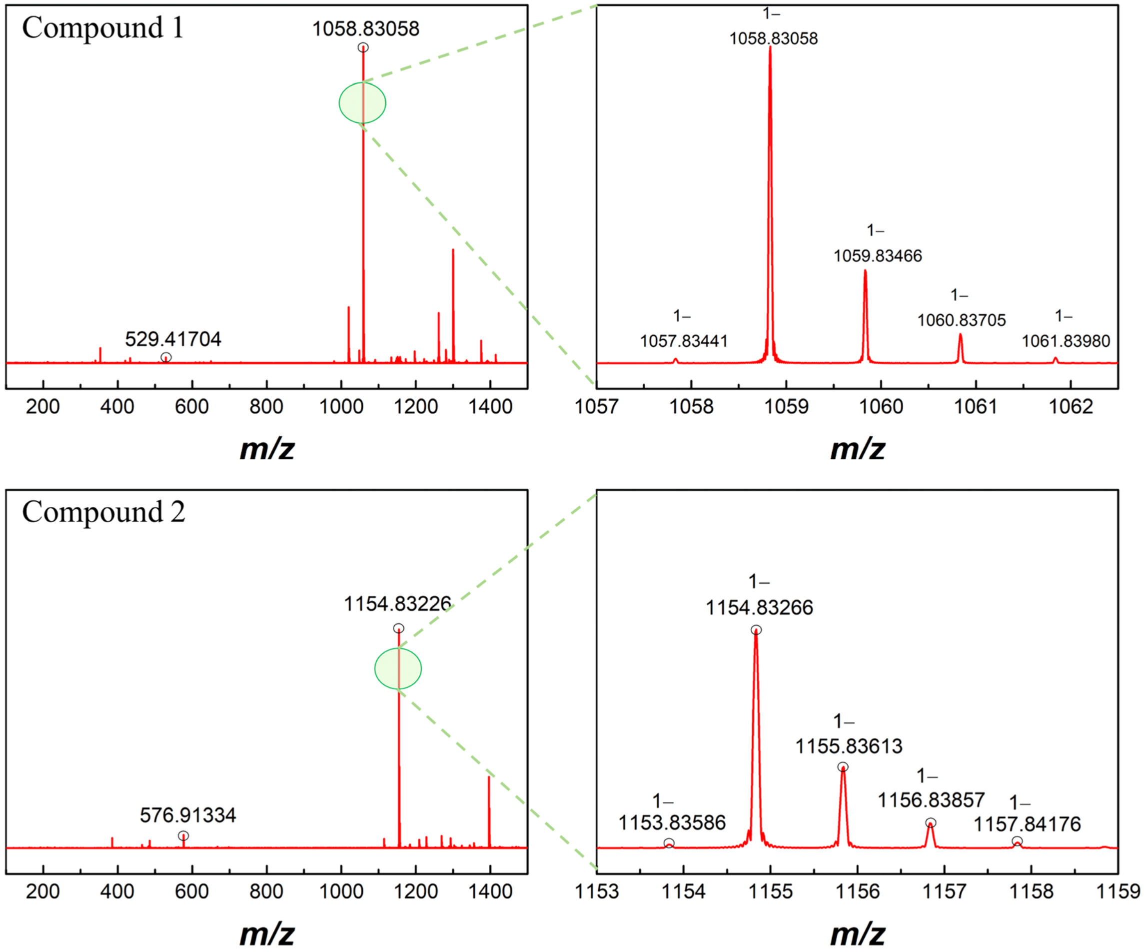

Figure 5 High-resolution electrospray ionization mass spectrum of compounds 1 and 2 from 101.1 to 1500.0 m/z.

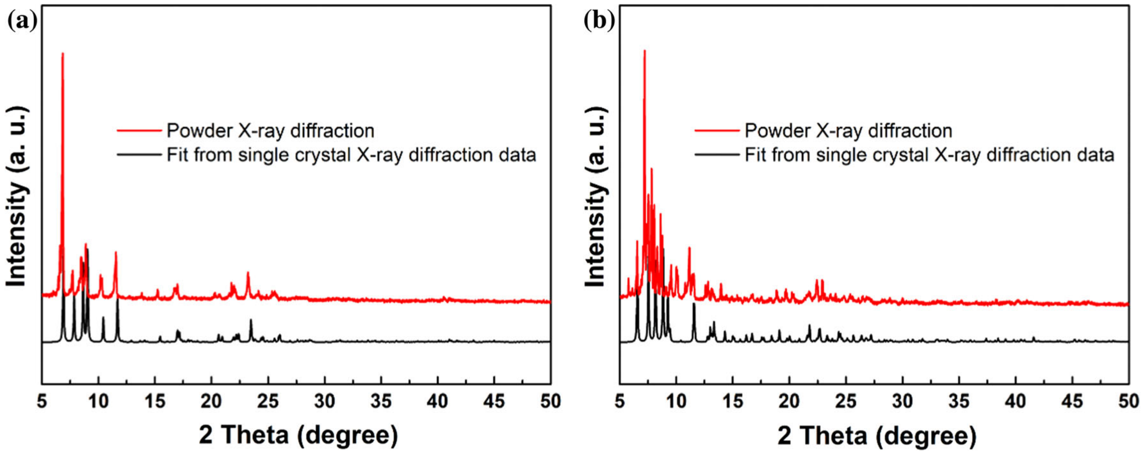

Figure 6 Powder X-ray diffraction patterns as well as the fitting patterns from the single-crystal X-ray diffraction data of compound 1 (**a**) and compound 2 (**b**), respectively.

area can facilitate the interactions between electrolytes and the active sites of electrocatalysts, as well as the electrons and ions. On the other hand, the small electrochemical active surface areas of POV parent and compound 1 were in accord with their HER rate-limiting step that chemisorbed hydrogen

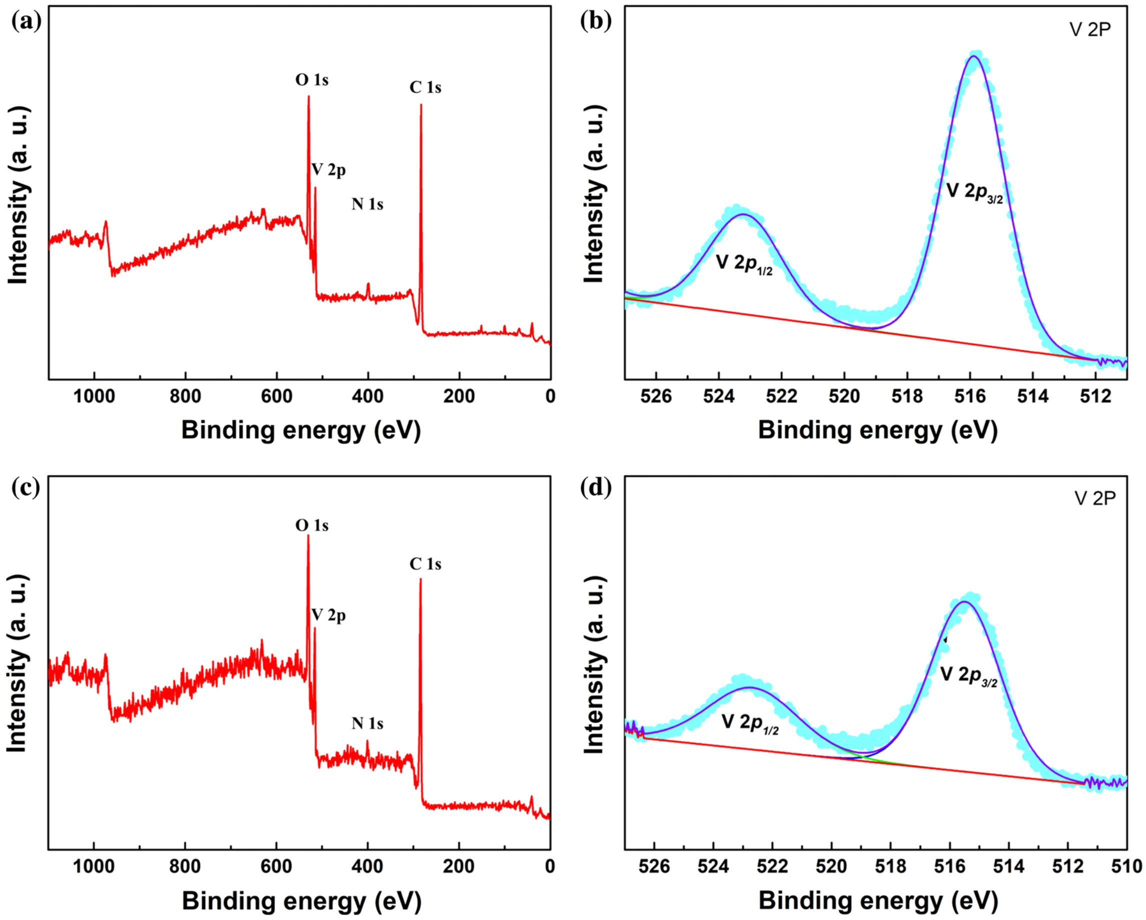

Figure 7 XPS spectra of compounds 1 (**a**, **b**) and 2 (**c**, **d**) (light blue points: testing curves, purple lines: fitting curves).

was the slowest process during electrocatalytic reaction. Hence, compound 2 incorporated with rigid bridging ligand can deliver improved electrocatalytic performance.

Conclusions

In this paper, we investigated the influences from the flexible/rigid bridging ligands to the non-covalent interactions, architectures, and the properties of POM-based inorganic–organic hybrid materials for the first time. We selected Lindqvist-type POV as the platform, succinyl or phthalyl group as bridging ligand, and cyclopropylamine with a stable configuration as the terminal ligand. By virtue of single crystal X-ray diffraction, the structures of the obtained hybrids were determined and discussed on atomic level. Interesting supramolecular assemblies originating from the intermolecular hydrogen bonds between the N atoms (amide groups) and the O atoms ($V\text{-}O_{terminal}$) arranged the polyanions into 1D chain-like architectures, which was only observed in POV hybrid containing rigid bridging ligand, while POV hybrid containing flexible bridging ligand did not exhibit any hydrogen bond. We applied molecular simulations and energy calculations to discuss the differences of packing structures between these two hybrids. After summarizing the reported POV hybrid materials with the same bridging ligands and analysing the ligand–architecture relationship, we draw a conclusion that rigid bridging ligand possesses a much stronger tendency to form intermolecular interactions than flexible ligand. To study the relationship between such interactions and the electrochemical properties of the hybrid materials, we applied the two compounds as electrocatalysts for HER and the results indicated that rigid bridging ligand delivered enhanced electrochemical properties than that of flexible one. This work demonstrated that the choice of bridging ligands could be a key to adjust the supramolecular architectures of POM-derived

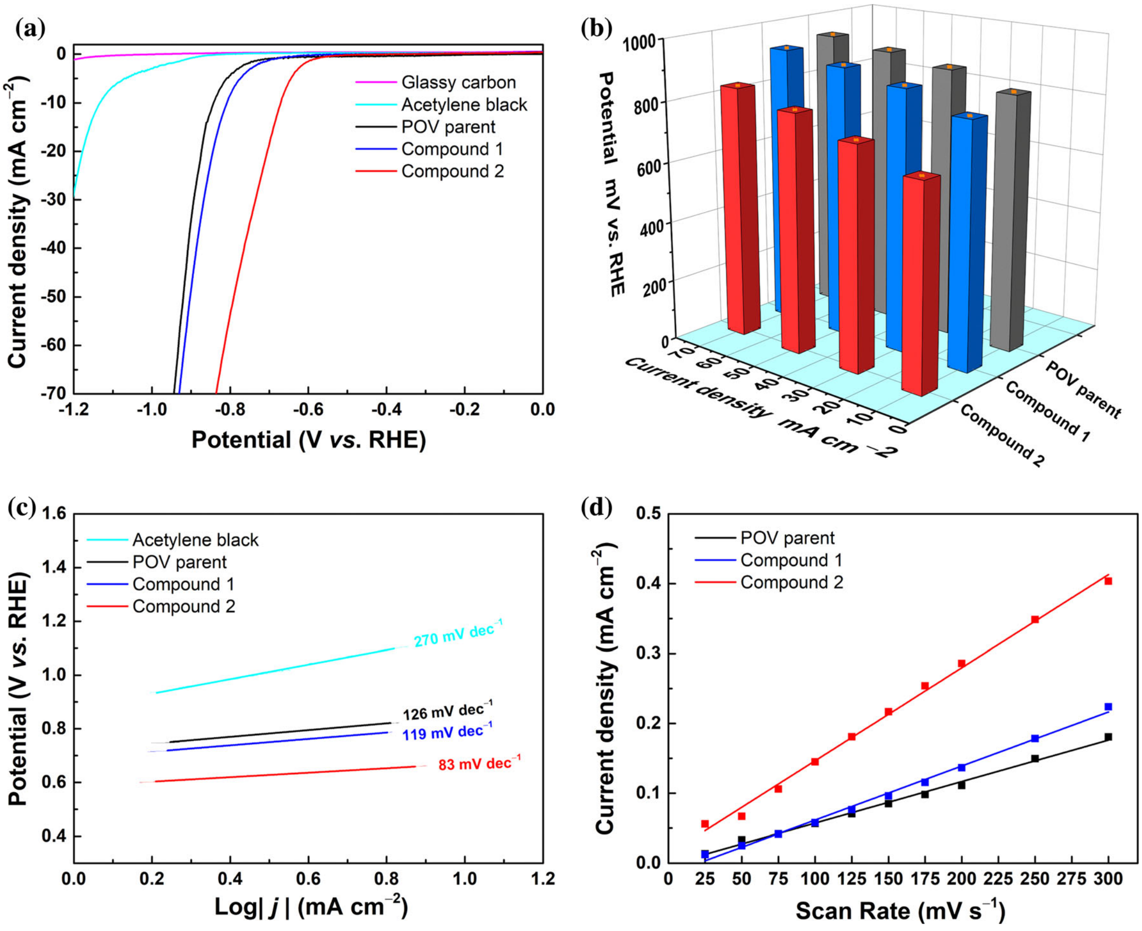

Figure 8 **a** LSV curves of black glassy carbon electrode, acetylene black, POV parent, compound 1 and compound 2, respectively. **b** Overpotential of POV parent, compound 1, and compound 2 at different current density. **c** Tafel slopes of POV parent, compound 1, and compound 2. **d** electrochemical active surface area of POV parent, compound 1, and compound 2 evaluated by C_{dl} values at different scan rates.

"Lego" toys, which will be beneficial to the design of POM hybrid materials, and also give a new idea for promising non-noble electrocatalysts for HER.

Acknowledgements

We appreciate the kind help from Juanjuan Han, Institute of Chemistry, Chinese Academy of Sciences, for the characterizations of HR-ESI–MS. This work is supported by National Natural Science Foundation of China (No. 21271068, 21401050), the Natural Science Foundation of Hubei Province (No. 2015CFA131), and Wuhan Applied Basic Research Program (No. 2014010101010020).

Author contributions

B. Huang, P. Wu, Z. Xiao, M. Liang, and P. Jiang provided the idea of this work. B. Huang, D. Ke conducted the experiments. B. Huang, D. Ke, Z. Xiao, and P. Wu conducted and analysed the single-crystal X-ray diffraction data, molecular simulation, and energy calculation. B. Huang, D. Ke, Z. Xiong, Y. Wang, K. Hu, M. Liang, P. Jiang conducted and analysed the spectroscopic characterizations.

Electrochemical tests were conducted by B. Huang, M. Liang, and P. Jiang. All authors have contributed themselves to the organization of the manuscript. B. Huang and D. Ke contributed equally to this work.

Compliance with ethical standards

Conflicts of interest The authors declare no conflict of interest.

Electronic supplementary material: The online version of this article (https://doi.org/10.1007/s10853-020-04404-0) contains supplementary material, which is available to authorized users.

References

[1] Liu T, Diemann E, Li H, Dress AWM, Müller A (2003) Self-assembly in aqueous solution of wheel-shaped Mo154 oxide clusters into vesicles. Nature 426(6962):59–62. https://doi.org/10.1038/nature02036

[2] Chen L, Chen W-L, Wang X-L, Li Y-G, Su Z-M, Wang E-B (2019) Polyoxometalates in dye-sensitized solar cells. Chem Soc Rev 48(1):260–284. https://doi.org/10.1039/c8cs00559a

[3] Fang W-H, Zhang L, Zhang J (2018) Synthetic strategies, diverse structures and tuneable properties of polyoxo-titanium clusters. Chem Soc Rev 47(2):404–421. https://doi.org/10.1039/c7cs00511c

[4] Bhagwan J, Khaja Hussain S, Yu JS (2020) Aqueous asymmetric supercapacitors based on $ZnCo_2O_4$ nanoparticles via facile combustion method. J Alloy Compd 815:152456. https://doi.org/10.1016/j.jallcom.2019.152456

[5] Duros V, Grizou J, Xuan W, Hosni Z, Long D-L, Miras HN, Cronin L (2017) Human versus robots in the discovery and crystallization of gigantic polyoxometalates. Angewandte Chemie-Int Ed 56(36):10815–10820. https://doi.org/10.1002/anie.201705721

[6] Xuan W, Pow R, Long D-L, Cronin L (2017) Exploring the molecular growth of two gigantic half-closed polyoxometalate clusters Mo180 and {Mo130Ce6}. Angewandte Chemie-Int Ed 56(33):9727–9731. https://doi.org/10.1002/anie.201702957

[7] Xuan W, Pow R, Watfa N, Zheng Q, Surman AJ, Long D-L, Cronin L (2019) Stereoselective assembly of gigantic chiral molybdenum blue wheels using lanthanide ions and amino acids. J Am Chem Soc 141(3):1242–1250. https://doi.org/10.1021/jacs.8b09750

[8] Mitchell SG, Streb C, Miras HN, Boyd T, Long DL, Cronin L (2010) Face-directed self-assembly of an electronically active Archimedean polyoxometalate architecture. Nat Chem 2(4):308–312. https://doi.org/10.1038/nchem.581

[9] Ishiba K, Noguchi T, Iguchi H, Morikawa M-a, Kaneko K, Kimizuka N (2017) photoresponsive nanosheets of polyoxometalates formed by controlled self-assembly pathways. Angewandte Chemie-Int Ed 56(11):2974–2978. https://doi.org/10.1002/anie.201612473

[10] Wang Y-R, Huang Q, He C-T, Chen Y, Liu J, Shen F-C, Lan Y-Q (2018) Oriented electron transmission in polyoxometalate-metalloporphyrin organic framework for highly selective electroreduction of CO_2. Nat Commun. https://doi.org/10.1038/s41467-018-06938-z

[11] Tian J, Xu Z-Y, Zhang D-W, Wang H, Xie S-H, Xu D-W, Ren Y-H, Wang H, Liu Y, Li Z-T (2016) Supramolecular metal-organic frameworks that display high homogeneous and heterogeneous photocatalytic activity for H_2 production. Nat Commun. https://doi.org/10.1038/ncomms11580

[12] Chen L, Luque R, Li Y (2017) Controllable design of tunable nanostructures inside metal-organic frameworks. Chem Soc Rev 46(15):4614–4630. https://doi.org/10.1039/c6cs00537c

[13] Du Y, Liu J-w, Shao C-y, Yang L-r (2019) Synthesis and characterization of luminescent metal–organic frameworks for the selective recognition of Cu^{2+} cation and Tryptophan. J Alloy Compd 781:904–912. https://doi.org/10.1016/j.jallcom.2018.12.157

[14] Huang Y, Sun Y, Zheng X, Aoki T, Pattengale B, Huang J, He X, Bian W, Younan S, Williams N, Hu J, Ge J, Pu N, Yan X, Pan X, Zhang L, Wei Y, Gu J (2019) Atomically engineering activation sites onto metallic 1T-MoS_2 catalysts for enhanced electrochemical hydrogen evolution. Nat Commun. https://doi.org/10.1038/s41467-019-08877-9

[15] Zhang J, Huang Y, Li G, Wei Y (2019) Recent advances in alkoxylation chemistry of polyoxometalates: from synthetic strategies, structural overviews to functional applications. Coord Chem Rev 378:395–414. https://doi.org/10.1016/j.ccr.2017.10.025

[16] Zhang H, Liu W, Li A, Zhang D, Li X, Zhai F, Chen L, Chen L, Wang Y, Wang S (2019) Three mechanisms in one material: uranium capture by a polyoxometalate-organic framework through combined complexation, chemical reduction, and photocatalytic reduction. Angew Chem Int Ed Engl. https://doi.org/10.1002/anie.201909718

[17] Zheng Q, Kupper M, Xuan W, Oki H, Tsunashima R, Long D-L, Cronin L (2019) Anisotropic polyoxometalate cages assembled via layers of heteroanion templates. J Am Chem Soc 141(34):13479–13486. https://doi.org/10.1021/jacs.9b04533

[18] Marrot J, Pilette MA, Haouas M, Floquet S, Taulelle F, Lopez X, Poblet JM, Cadot E (2012) Polyoxometalates

paneling through Mo2O2S2 coordination: cation-directed conformations and chemistry of a supramolecular hexameric scaffold. J Am Chem Soc 134(3):1724–1737. https://doi.org/10.1021/ja2090383

[19] Yin P, Wu P, Xiao Z, Li D, Bitterlich E, Zhang J, Cheng P, Vezenov DV, Liu T, Wei Y (2011) A double-tailed fluorescent surfactant with a hexavanadate cluster as the head group. Angew Chem Int Ed Engl 50(11):2521–2525. https://doi.org/10.1002/anie.201006144

[20] Song Y-F, McMillan N, Long D-L, Kane S, Malm J, Riehle MO, Pradeep CP, Gadegaard N, Cronin L (2009) Micropatterned surfaces with covalently grafted unsymmetrical polyoxometalate-hybrid clusters lead to selective cell adhesion. J Am Chem Soc 131(4):1340–1341. https://doi.org/10.1021/ja807091v

[21] Huang B, Wang N, Yang K, Ke D, Fang Y, Hu X, Wu B, Xiao Z, Wu P, Wei Y (2018) Stepwise syntheses and supramolecular assemblies of a series of polyoxovanadate hybrids with various architectures. New J Chem 42(8):5853–5858. https://doi.org/10.1039/c7nj04727d

[22] Zhang L, Liu X, Sun F, Jian J, Sun X, Wu D, Yuan H (2019) Proton conducting in a new vanadoborate with 3D structure through hydrogen bonding. J Alloy Compd. https://doi.org/10.1016/j.jallcom.2019.152505

[23] He J, Li J, Du W, Han Q, Wang Z, Li M (2018) A mesoporous metal-organic framework: potential advances in selective dye adsorption. J Alloy Compd 750:360–367. https://doi.org/10.1016/j.jallcom.2018.03.393

[24] Stuckart M, Monakhov KY (2019) Polyoxometalates as components of supramolecular assemblies. Chem Sci 10(16):4364–4376. https://doi.org/10.1039/C9SC00979E

[25] Li C, Mizuno N, Yamaguchi K, Suzuki K (2019) Self-assembly of anionic polyoxometalate-organic architectures based on lacunary phosphomolybdates and pyridyl ligands. J Am Chem Soc 141(19):7687–7692. https://doi.org/10.1021/jacs.9b02541

[26] Yi X, Izarova NV, Stuckart M, Guerin D, Thomas L, Lenfant S, Vuillaume D, van Leusen J, Duchon T, Nemsak S, Bourone SDM, Schmitz S, Koegerler P (2017) Probing frontier orbital energies of Co9(P2W15)3 polyoxometalate clusters at molecule-metal and molecule-water interfaces. J Am Chem Soc 139(41):14501–14510. https://doi.org/10.1021/jacs.7b07034

[27] Zhang J, Zhao Z, Zhang J, She S, Huang Y, Wei Y (2014) Spontaneous resolution of polyoxometalate-based inorganic-organic hybrids driven by solvent and common ion. Dalton Trans 43(46):17296–17302. https://doi.org/10.1039/c4dt01954g

[28] Liu S-M, Zhang Z, Li X-H, Jia H-J, Liu S-X (2018) Synthesis and photophysical properties of crystalline [EuW10O36]9–based polyoxometalates with lanthanide ions as counter cations. J Alloy Compd 761:52–57. https://doi.org/10.1016/j.jallcom.2018.05.144

[29] Xu X, Spasojevic-de Bire A, Ghermani NE, Wei Y, Novakovic S, Bosnjakovic-Pavlovic N, Wu P (2017) Experimental evidence of charge transfer in a functionalized hexavanadate: a high resolution X-ray diffraction study. Phys Chem Chem Phys 19(28):18162–18166. https://doi.org/10.1039/C7CP01840A

[30] Yvon C, Surman AJ, Hutin M, Alex J, Smith BO, Long D-L, Cronin L (2014) Polyoxometalate clusters integrated into peptide chains and as inorganic amino acids: solution- and solid-phase approaches. Angew Chem Int Ed 53(13):3336–3341. https://doi.org/10.1002/anie.201311135

[31] Hu X, Wang H, Huang B, Li N, Hu K, Wu B, Xiao Z, Wei Y, Wu P (2019) A new scheme for rational design and synthesis of polyoxovanadate hybrids with high antitumor activities. J Inorg Biochem 193:130–132. https://doi.org/10.1016/j.jinorgbio.2019.01.013

[32] Hutin M, Yvon C, Yan J, Macdonell A, Long D-L, Cronin L (2013) Programming the assembly of carboxylic acid-functionalised hybrid polyoxometalates. CrystEngComm 15(22):4422–4430. https://doi.org/10.1039/C3CE26816K

[33] Huang B, Xiao Z, Wu B, Hu X, Hu X, Wu P, Wei Y (2017) Synthesis, crystal structure and spectroscopic studies of a series of hexavanadate hybrids with multiple functional groups. Inorg Chem Front 4(1):165–170. https://doi.org/10.1039/c6qi00302h

[34] Monakhov KY, Bensch W, Koegerler P (2015) Semimetal-functionalised polyoxovanadates. Chem Soc Rev 44(23):8443–8483. https://doi.org/10.1039/c5cs00531k

[35] Li J-K, Dong J, Wei C-P, Yang S, Chi Y-N, Xu Y-Q, Hu C-W (2017) Controllable synthesis of lindqvist alkoxopolyoxovanadate clusters as heterogeneous catalysts for sulfoxidation of sulfides. Inorg Chem 56(10):5748–5756. https://doi.org/10.1021/acs.inorgchem.7b00366

[36] Wang K, He Y, Zhao Y, Ma P, Wang J (2019) A propionate-functionalized polyoxovanadate K2[V10O16(OH)6(CH3CH2CO2)6]·20H2O: as catalyst for degradation of methylene blue. J Mol Struct 1195:184–188. https://doi.org/10.1016/j.molstruc.2019.05.130

[37] Taleghani S, Mirzaei M, Eshtiagh-Hosseini H, Frontera A (2016) Tuning the topology of hybrid inorganic–organic materials based on the study of flexible ligands and negative charge of polyoxometalates: a crystal engineering perspective. Coord Chem Rev 309:84–106. https://doi.org/10.1016/j.ccr.2015.10.004

[38] Anyushin AV, Kondinski A, Parac-Vogt TN (2019) Hybrid polyoxometalates as post-functionalization platforms: from

fundamentals to emerging applications. Chem Soc Rev. https://doi.org/10.1039/c8cs00854j

[39] Ji Y, Huang L, Hu J, Streb C, Song Y-F (2015) Polyoxometalate-functionalized nanocarbon materials for energy conversion, energy storage and sensor systems. Energy Environ Sci 8(3):776–789. https://doi.org/10.1039/c4ee03749a

[40] Ge J, Hu J, Zhu Y, Zeb Z, Zang D, Qin Z, Huang Y, Zhang J, Wei Y (2019) Recent advances in polyoxometalates for applications in electrocatalytic hydrogen evolution reaction. Acta Phys Chim Sin 36(1):1906060–1906063. https://doi.org/10.3866/pku.whxb201906063

[41] Xiao Z, Chen K, Wu B, Li W, Wu P, Wei Y (2016) An easy way to construct polyoxovanadate-based organic-inorganic hybrids by stepwise functionalization. Eur J Inorg Chem 6:808–811. https://doi.org/10.1002/ejic.201501297

[42] Wu P, Xiao Z, Zhang J, Hao J, Chen J, Yin P, Wei Y (2011) DMAP-catalyzed esterification of pentaerythritol-derivatized POMs: a new route for the functionalization of polyoxometalates. Chem Commun (Camb) 47(19):5557–5559. https://doi.org/10.1039/c1cc10650c

[43] Santoni M-P, Pal AK, Hanan GS, Tang M-C, Venne K, Furtos A, Menard-Tremblay P, Malveau C, Hasenknopf B (2012) Coordination-driven self-assembly of polyoxometalates into discrete supramolecular triangles. Chem Commun 48(2):200–202. https://doi.org/10.1039/c1cc16155e

[44] Raizada M, Sama F, Ashafaq M, Shahid M, Ahmad M, Siddiqi ZA (2017) New hybrid polyoxovanadate–Cu complex with V···H interactions and dual aqueous-phase sensing properties for picric acid and Pd^{2+}: x-ray analysis, magnetic and theoretical studies, and mechanistic insights into the hybrid's sensing capabilities. J Mater Chem C 5(36):9315–9330. https://doi.org/10.1039/C7TC03172F

[45] Zhang Y, Wang X, Li S, Song B, Shao K, Su Z (2016) Ligand-directed assembly of polyoxovanadate-based metal-organic polyhedra. Inorg Chem 55(17):8770–8775. https://doi.org/10.1021/acs.inorgchem.6b01338

[46] Kastner K, Streb C (2013) Solvent-shielding allows the self-assembly of supramolecular 1D barium vanadate chains. CrystEngComm 15(24):4948–4955. https://doi.org/10.1039/C3CE40536B

[47] Lin X, Huang B, Xiong Z, Fang T, Zhang X, Xiao Z, Wu P (2018) Supramolecular architectures of polyoxometalate hybrids originating from halogen and hydrogen-bonding interactions. ChemistrySelect 3(39):11008–11011. https://doi.org/10.1002/slct.201802912

[48] Huang B, Xiao Z, Wang Y, Ke D, Zhu C, Zhang S, Hu X, Wu P (2019) Destroy the inherent symmetry of vanadium-based inorganic cluster through chiral organic ligand: synthesis and characterization of a polyoxovanadate-derived amino acid ester hybrid. J Mol Struct 1195:10–16. https://doi.org/10.1016/j.molstruc.2019.05.114

[49] Wilson EF, Miras HN, Rosnes MH, Cronin L (2011) Real-time observation of the self-assembly of hybrid polyoxometalates using mass spectrometry. Angew Chem Int Ed Engl 50(16):3720–3724. https://doi.org/10.1002/anie.201006938

[50] Fernandes DM, Barbosa ADS, Pires J, Balula SS, Cunha-Silva L, Freire C (2013) Novel composite material Polyoxovanadate@MIL-101(Cr): a highly efficient electrocatalyst for ascorbic acid oxidation. ACS Appl Mater Interfaces 5(24):13382–13390. https://doi.org/10.1021/am4042564

[51] Chen H-Y, Wee G, Al-Oweini R, Friedl J, Tan KS, Wang Y, Wong CL, Kortz U, Stimming U, Srinivasan M (2014) A polyoxovanadate as an advanced electrode material for supercapacitors. ChemPhysChem 15(10):2162–2169. https://doi.org/10.1002/cphc.201400091

[52] VanGelder LE, Petel BE, Nachtigall O, Martinez G, Brennessel WW, Matson EM (2018) Organic functionalization of polyoxovanadate-alkoxide clusters: improving the solubility of multimetallic charge carriers for nonaqueous redox flow batteries. Chemsuschem 11(23):4139–4149. https://doi.org/10.1002/cssc.201802029

[53] Hartung S, Bucher N, Chen HY, Al-Oweini R, Sreejith S, Borah P, Zhao Y, Kortz U, Stimming U, Hoster HE, Srinivasan M (2015) Vanadium-based polyoxometalate as new material for sodium-ion battery anodes. J Power Sources 288:270–277. https://doi.org/10.1016/j.jpowsour.2015.04.009

[54] Chao L, Kai Z, Yuan W (2017) Catalytic properties of platinum nanoclusters supported on iron oxides for the solvent-free hydrogenation of halonitrobenzene. Acta Phys Chim Sin 33(5):984–992. https://doi.org/10.3866/pku.whxb201702084

[55] Li X-X, Zhang L-J, Cui C-Y, Wang R-H, Yang G-Y (2018) Designed construction of cluster organic frameworks from lindqvist-type polyoxovanadate cluster. Inorg Chem 57(16):10323–10330. https://doi.org/10.1021/acs.inorgchem.8b01528

[56] Bai Y, Yan Z, Kang L, Liu Z-H (2019) Preparation and capacitance of V2O5/holey graphene hybrid aerogel electrode with high performance. J Alloy Compd 780:792–799. https://doi.org/10.1016/j.jallcom.2018.12.006

[57] Linnenberg O, Kondinski A, Stocker C, Monakhov KY (2017) The Cu(i)-catalysed Huisgen 1,3-dipolar cycloaddition route to (bio-)organic functionalisation of polyoxovanadates. Dalton Trans 46(45):15636–15640. https://doi.org/10.1039/C7DT03376A

[58] Linnenberg O, Mayerl L, Monakhov KY (2018) The Heck reaction as a tool to expand polyoxovanadates towards thiol-

sensitive organic–inorganic hybrid fluorescent switches. Dalton Trans 47(41):14402–14407. https://doi.org/10.1039/C8DT02340A

[59] Hu X, Xiao Z, Huang B, Hu X, Cheng M, Lin X, Wu P, Wei Y (2017) Syntheses and post-functionalization of tri-substituted polyalkoxohexavanadates containing tris(alkoxo) ligands. Dalton Trans 46(26):8505–8513. https://doi.org/10.1039/c7dt01543g

[60] Huang B, Hu X, Hu X, Wang N, Yang K, Xiao Z, Wu P (2017) Synthesis and characterization of a novel inorganic-organic hybrid material based on polyoxometalates and dicyclohexylcarbodiimide. J Mol Struct 1149:42–47. https://doi.org/10.1016/j.molstruc.2017.07.088

[61] Shen J-Q, Zhang Y, Zhang Z-M, Li Y-G, Gao Y-Q, Wang E-B (2014) Polyoxoniobate-based 3D framework materials with photocatalytic hydrogen evolution activity. Chem Commun 50(45):6017–6019. https://doi.org/10.1039/c3cc49245a

[62] Sullivan KP, Neiwert WA, Zeng H, Mehta AK, Yin Q, Hillesheim DA, Vivek S, Yin P, Collins-Wildman DL, Weeks ER, Liu T, Hill CL (2017) Polyoxometalate-based gelating networks for entrapment and catalytic decontamination. Chem Commun 53(83):11480–11483. https://doi.org/10.1039/c7cc05657e

[63] Gong Y-R, Chen W-C, Zhao L, Shao K-Z, Wang X-L, Su Z-M (2018) Functionalized polyoxometalate- based metalorganic cuboctahedra for selective adsorption toward cationic dyes in aqueous solution. Dalton Trans 47(37):12979–12983. https://doi.org/10.1039/c8dt02580k

[64] Li S, Zhang L, Lu B, Yan E, Wang T, Li L, Wang J, Yu Y, Mu Q (2018) A new polyoxovanadate-based metal-organic framework: synthesis, structure and photo-/electro-catalytic properties. New J Chem 42(9):7247–7253. https://doi.org/10.1039/c7nj05032a

[65] Amiinu IS, Pu Z, Liu X, Owusu KA, Monestel HGR, Boakye FO, Zhang H, Mu S (2017) Multifunctional Mo-N/C@MoS2 electrocatalysts for HER, OER, ORR, and Zn-Air batteries. Adv Func Mater 27(44):1702300. https://doi.org/10.1002/adfm.201702300

[66] Tang Y-J, Gao M-R, Liu C-H, Li S-L, Jiang H-L, Lan Y-Q, Han M, Yu S-H (2015) Porous molybdenum-based hybrid catalysts for highly efficient hydrogen evolution. Angew Chem Int Ed 54(44):12928–12932. https://doi.org/10.1002/anie.201505691

[67] Jing S, Zhang L, Luo L, Lu J, Yin S, Shen PK, Tsiakaras P (2018) N-doped porous molybdenum carbide nanobelts as efficient catalysts for hydrogen evolution reaction. Appl Catal B 224:533–540. https://doi.org/10.1016/j.apcatb.2017.10.025